Chinese Journal of
POLYMER SCIENCE

RESEARCH ARTICLE

https://doi.org/10.1007/s10118-026-3783-6
Chinese J. Polym. Sci.

Phase Equilibrium Analysis of Ternary Systems Based on an Epoxy Oligomer, Polysulfone, and Tetraethoxysilane

Ivan M. Obidin, Maria V. Mironova, and Ivan Yu. Skvortsov*

A.V. Topchiev Institute of Petrochemical Synthesis, Russian Academy of Sciences, Moscow 119991, Russian Federation

Abstract Phase equilibria were investigated in uncured mixtures composed of an epoxy oligomer, polysulfone, and tetraethoxysilane. Pairwise interaction parameters were calculated and binodal curves were constructed. The mutual diffusion coefficients of the components were determined and the influence of tetraethoxysilane on the diffusion processes in both binary and ternary systems was examined. Phase diagrams of the binary and ternary systems were established using optical microscopy and dynamic light scattering, and the boundary compositions corresponding to the single-phase region were identified.

Keywords Epoxy; Polysulfone; Tetraethoxysilane; Phase equilibrium; Interdiffusion

Citation: Obidin, I. M.; Mironova, M. V.; Skvortsov, I. Y. Phase equilibrium analysis of ternary systems based on an epoxy oligomer, polysulfone, and tetraethoxysilane. *Chinese J. Polym. Sci.* https://doi.org/10.1007/s10118-026-3783-6

INTRODUCTION

Epoxy oligomers (EOs) remain among the most popular binders for composite material production. The prevalence of epoxy resins is attributed to their unique physicochemical and technological properties.[1–5] However, to obtain materials with the required combination of strength, wear resistance, and heat resistance, epoxy matrices must be modified.[6–11]

Well-known modifiers of epoxy resins are thermoplastic polymers such as polyetheretherketones,[12–14] polyethersulfones,[15,16] and polyetherimides.[17–19] Thermoplastic modifiers significantly improve the thermomechanical characteristics of cured compositions and can impart specific properties to the final product, such as increased crack resistance, chemical resistance, and improved adhesive strength.[12–14,17–20] Polysulfone (PSF) is a common thermoplastic used to modify epoxy oligomers based on bisphenol A.[21–23]

Several authors have demonstrated an increase in the impact toughness of composites based on EO and PSF, while maintaining the thermal stability of the material.[21,22] However, a decrease in the flexural strength was noted. Sun *et al*. found that with an increase in the PSF content, an increase in the fracture toughness parameter of the composite by almost two times was observed compared with the unfilled EO.[22]

The use of modifiers, particularly polysulfones, can lead to an increase in the mixture viscosity, which affects the processing conditions of the product and limits its applicability (for example, as an impregnation of fibers). Low-molecular weight diluents are typically used to reduce the viscosity of binders. Such components reduce the viscosity of the system at the stage of obtaining the composite and add functional properties to the matrix after its curing.[24,25] In a number of studies, alkyl glycidyl ether,[24,26,27] furfuryl glycidyl ether,[25] diethylene glycol,[28] and 1,2-cyclohexanediol diglycidyl ether,[29] have been considered as active diluents. Thus, owing to their structure, glycidyl ethers can be incorporated into the polyepoxy network by reducing the viscosity of the uncured system, improving adhesion with discrete fibers, and increasing the elasticity of the cured composite.[27,30–33]

Kurbatov V.G. *et al*. introduced furfuryl glycidyl ether into the EO system with PSF, which led to a significant decrease in binder viscosity.[32] The glass transition temperature of the cured epoxy polysulfone mixtures remained virtually unchanged with the introduction of the active diluent, FGE. The authors demonstrated the possibility of reducing the viscosity of the binder while maintaining a high modifier content to ensure the crack resistance of the matrices and reinforced plastics based on them. Qiao *et al*. introduced alkyl glycidyl ether into EO and cured this mixture using two different hardeners.[27] The greatest effect on viscosity reduction was observed with the introduction of up to 10% active diluent, while maintaining the high mechanical properties of the cured composites.

Orthosilicic acid esters and ethyl silicates are a class of active EO diluents.[34–38] Because of their low intrinsic viscosity and limited compatibility with EO, these components contribute to a significant reduction in the viscosity of mixtures during processing into products, followed by transformation into oligosiloxanes. A characteristic feature of this type of substance is the formation of silicon dioxide particles with a

* Corresponding author, E-mail: iskvortsov@ips.ac.ru
Received April 8, 2026; Accepted June 11, 2026; Published online September 1, 2026

uniform distribution throughout the volume owing to the in situ hydrolytic polycondensation reaction in a thermosetting matrix.[35,39–41]

Recent studies on binary and ternary polymer blends have demonstrated complex phase behavior governed by thermodynamic incompatibility and kinetic stabilization effects. In particular, the role of the third component in tuning the miscibility windows and controlling the phase separation pathways has been widely reported.[42,43]

The inclusion of tetraethoxysilane (TEOS) in a PSF/EO solution is of interest to obtain composites with a developed interphase surface and the possibility of obtaining PSF-concentrated compositions with low viscosity for possible use as impregnating binders in the preparation of continuous fiber-based prepregs, including those suitable for 3D printing.

However, high concentrations of diluents can lead to a decrease in the strength of composites and deterioration in their thermal stability, as shown in articles.[27,30–33] A low-molecular-weight component can cause stratification of the mixture, making it unsuitable for processing. Therefore, for ternary epoxy oligomer/diluent/modifier systems, component compatibility is an important issue. The study of phase equilibria in ternary systems will make it possible to predict and control the multicomponent curable composition structure and properties. The main objectives of this study were to analyze the mutual solubility of the EO/TEOS/PSF ternary system components, calculate the paired interaction parameters, and construct a ternary phase diagram.

EXPERIMENTAL

Materials

An epoxy oligomer based on bisphenol A (ED-20, Armplast, Russian Federation) was used as the epoxy binder. The degree of polymerization was n=1–4, M_w=390 g/mol. Polysulfone with M_w=3.5×10^4 g/mol (PSK-1, Joint-Stock Company G.S. Petrov Institute of Plastics, Moscow, Russia) was used as a thermoplastic modifier. Tetraethoxysilane (special purity grade, 99.9% purity; EKOS-1, Russia) was used as the organosilicon modifier.

To analyze the compatibility of the systems, binary mixtures of TEOS in EO (TEOS concentration range of 15 vol%–90 vol%, 5 vol% increments), PSF solutions in EO (PSF concentrations of 5 vol%, 10 vol%, and 15 vol%), and three-component EO/TEOS/PSF systems were prepared. All compositions were designated as EO/TEOS/PSF, TEOS/EO, and PSF/EO, with concentrations indicated as volume percentages (the volume fractions of EO, PSF, and TEOS sum to 100%).

Solutions and Emulsions Preparation

PSF was predried under vacuum for 4 h at a constant temperature of 110 °C. The epoxy oligomer was heated to 150 °C and PSF was gradually added until the polymer was completely dissolved. The resulting mixture was cooled to 100 °C, TEOS was added, and the mixture was stirred for 4 h.

Polysulfone films were prepared to study the samples by interferometry. The films were produced by casting[44,45] from a 5% polymer solution in dichloroethane. The samples were dried at room temperature and then stored in a drying oven at 85 °C until constant weight was reached. The thickness of the film was 60 μm.

The Cloud Point Method (Dynamic Light Scattering)

The phase states of the mixtures were measured using a Zetasizer Nano Photoanalyzer (Malvern Instruments, England). The turbidity-onset temperature of the TEOS/EO mixtures was determined from the change in the intensity of light scattered at an angle of 173° and detected at a fixed focusing position (3 mm). Before testing, the prepared mixtures were heated by stirring at 90 °C (above the upper critical mixing temperature) to obtain a transparent homogeneous solution. One milliliter of the solution was poured into a heated quartz cuvette, and the cuvette was placed in the analyzer cell. The experiment was carried out in cooling and heating modes in the temperature range of 0–90 °C with a step of 1 °C. The sample was equilibrated at each temperature for 1 min, followed by signal accumulation (1 min per point). To prevent separation of the low-viscosity emulsion (in the case of tests under heating), the experiment was carried out by stirring the sample immediately before measurement for each temperature.

Optical Microscopy

The morphology of the resulting mixtures was studied using a Biomed 6 PO optical microscope (Russia). A drop of the mixture was placed on a glass slide and pressed with a coverslip to reduce the risk of atmospheric moisture ingress and TEOS evaporation. The samples were heated from room temperature (25 °C) to 200 °C. Changes in the morphology of the solution droplet upon cooling were studied in the temperature range from 100 °C to 30 °C. A Mettler Toledo FP900 thermal system equipped with an FP 82 hot stage (USA) was used in this study.

Optical Microinterferometry Method

The optical interferometry method was used to evaluate the interdiffusion of the components of the PSF/EO, TEOS/EO, and EO/TEOS/PSF systems.[46,47] The laboratory interferometer setup was constructed based on a POLAM L-213M microscope (Joint Stock Company "LOMO," Russia). A monochromatic laser with a wavelength of 532 nm was used as light source. The experiment was performed using a generally accepted technique.[48,49] The sample was placed in a wedge-shaped gap ($\alpha \leq 2°$) between two glass plates. A reflective coating based on titanium alloy was applied to the contact surfaces of the plates. The formation and changes in the interference pattern during the contact of the components were monitored. The systems of interference fringes with different pitches corresponded to the refractive indices of the components under study. Mutual diffusion of components leads to the emergence of a concentration gradient and, consequently, a gradient of refractive indices and curvature of the bands on both sides of the phase boundary.[50,51]

To study the two-component PSF/EO system, a PSF film was placed between the glasses and brought into contact with EO. To analyze the phase state of the three-component EO/TEOS/PSF system, a PSF solution in EO was brought into contact with TEOS. All experiments were carried out in the isothermal mode at a fixed temperature, as well as with stepwise heating, in the temperature range of 25–200 °C (depending on the system). At each stage, the system was maintained at a given temperature until equilibrium was reached for at least 30 min. Analysis of the obtained interference patterns allows the construction of concentration profiles of the components in the diffusion zone and the calculation of the interdiffusion coefficients of the components.

https://doi.org/10.1007/s10118-026-3783-6

RESULTS AND DISCUSSION

Theoretical Calculation of Compatibility Using the Hansen Method

The selection of a method for assessing component compatibility in complex systems is a key step in the development of polymer and composite materials. There are several empirical and semi-empirical methods of theoretical solubility that are widely used in polymer chemistry and materials science: the Hildebrand method is based on the energy required to break intermolecular interactions,[52–54] a method based on the Flory-Huggins thermodynamic model,[55,56] a Hansen method (Hansen Solubility Parameters, HSP),[57,58] and other experimental methods based on phase analysis. In this study, the Hansen method was used because it provides a deeper and physically sound description of the interactions between the components.[59,60] This method considers three independent types of intermolecular forces: dispersion interactions (δ_d), polar interactions (δ_p), and hydrogen bonds (δ_h). The solute is represented by the center of a sphere with radius R_0 in space, δ_d, δ_p, and δ_h. Solubility is estimated by the distance between the solute and solvent (R_a):

$$R_a^2 = 4 \cdot (\delta_{dp} - \delta_{ds})^2 + (\delta_{pp} - \delta_{ps})^2 + (\delta_{hp} - \delta_{hs})^2 \quad (1)$$

The index p refers to the polymer and the index s refers to the solvent.

Substances for which the δ values lie within this sphere are "good" solvents.[61,62] A "bad" solvent is located outside the radius of the polymer sphere. The ratio of the interaction radius (R_a) to the radius of the polymer solubility sphere (R_0) is known as the relative energy difference (RED). If R_a for a solvent is less than R_0 for a polymer, then this solvent is compatible with the polymer (RED<1). If R_a for a solvent is greater than R_0 for a polymer, then this solvent does not interact with the polymer (RED>1). The equality between R_a and R_0 is the solubility/insolubility boundary (RED=1).

The solubility of epoxy oligomers, such as that of polysulfones, has been studied in considerable detail,[23,26,32,50,63] while a search of the literature on the solubility parameters for various epoxy oligomers based on bisphenol A and epichlorohydrin yielded rather contradictory data on specific solubility parameters. The spread of published experimental data for PSF is also significant. Table 1 lists the solubility parameters for the epoxy matrix and polysulfone from various peer-reviewed sources (Table 1).

Among the various grades of materials studied, the choice was made in favor of PSU ULTRASON S and ED-20.

Based on the literature data obtained for the studied components (EO, PSF, and TEOS), the cohesive energies were calculated, and the RED parameters were determined. For the calculations, R_0 values of 8 $MPa^{0.5}$ for polysulfone[57] and 20.5 $MPa^{0.5}$ for EO[57] were used. Tables 2 and 3 list the calculation results. According to calculations for two-component systems, the PSF/EO pair has a RED value below unity, indicating the mutual compatibility of the components. Physically, this means that the energy required to mix the components is lower than the cohesive energy of each individual; therefore, the interaction between the polymer segments and oligomer molecules is thermodynamically favorable. For PSF and TEOS, RED>1 was found because of significant differences in the interaction parameters, primarily dispersion, indicating the incompatibility of these components. The RED values obtained for the TEOS/EO pair indicated a "good" affinity between the components (Table 3).

Based on the RED data for EO and TEOS in relation to PSF, a graph of the dependence of the solubility of PSF in a mixture of TEOS/EO solvents at different ratios was constructed (Fig. 1).

With a further increase in the TEOS content, the mixture

Table 1 Hansen solubility parameters for polysulfone and epoxy oligomer.

Epoxy oligomers					
Brand	Epoxy number	δ_d ($MPa^{0.5}$)	δ_p ($MPa^{0.5}$)	δ_h ($MPa^{0.5}$)	R_0
DGEBA[64]	0.25	17.15	6.92	8.22	–
Epikote 828[57]	0.185–0.192	23.10	14.60	5.00	–
E828[65]	0.19–0.2	17.02	8.34	8.85	–
ED-20[66]	0.19–0.225	19.79	5.06	5.21	20.5
DGEBA epoxy[67]	0.445–0.5*	20.7	5.6	10.8	–
Polysulfones					
Brand	$M_w \times 10^{-3}$	δ_d ($MPa^{0.5}$)	δ_p ($MPa^{0.5}$)	δ_h ($MPa^{0.5}$)	
PSU ULTRASON S[57]	62	19.70	8.30	8.3	8
PSU[57]		16	6	6.6	9
Polysulfone UDEL® P-3500[68]	77–86	18.38	16.48	7.49	–
Polysulfone Udel P-1700 NT 11[69]	22–32	19.02	5.90	6.13	–
PSU pellets Aldrich Chemical Co.[70]	35	18.50	8.50	7.00	9.4

* 75% in xylene.

Table 2 Hansen solubility parameter data for PSF with EO/TEOS.

Component	δ_d ($MPa^{0.5}$)	δ_p ($MPa^{0.5}$)	δ_h ($MPa^{0.5}$)	RED
PSF[57]	19.7	8.3	8.3	–
EO[66]	19.79	5.06	5.21	0.56
TEOS[57]	13.9	4.3	0.6	1.81

Table 3 Hansen solubility parameter data for EO with TEOS.

Component	δ_d (MPa$^{0.5}$)	δ_p (MPa$^{0.5}$)	δ_h (MPa$^{0.5}$)	RED
EO[66]	19.79	5.06	5.21	–
TEOS[57]	13.9	4.3	0.6	0.62

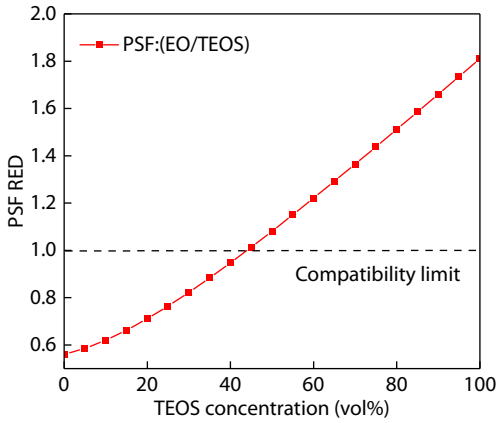

Fig. 1 Dependence of the relative energy difference for PSF on the composition of the TEOS/EO mixture. As can be seen from the presented dependence, at low TEOS concentrations in the mixture with EO, the RED value remains less than unity, indicating the preservation of the thermodynamic compatibility of the system. In this range, EO partially compensates for the differences in the thermodynamic compatibility parameters of PSF and TEOS and stabilizes the solution, preventing early phase separation.

solubility parameters gradually shifted away from those of PSF, especially in terms of δ_p and δ_h. As a result, the thermodynamic distance R_a increases, and because PSF has a relatively small solubility radius R_0 even a moderate increase in R_a produces a noticeable increase in the RED value. Therefore, although the δ differences change only gradually at low TEOS contents, the RED parameter increases steadily and crosses the miscibility threshold (RED=1) at approximately 45 vol% TEOS.

Upon reaching a critical concentration, when RED>1, the system enters the region of conditional thermodynamic instability, the intermolecular interactions of the PSF are no longer compensated by the presence of EO, and the formation of two phases in the mixture becomes energetically more favorable.

A significant result of the literature search and computational experiments was the relatively broad compatibility range of these systems. However, Hansen's computational method allowed for a significant narrowing of the concentration range for the subsequent compatibility experiments. Based on the calculations, compatibility ranges for the TEOS/EO and ternary EO/TEOS/PSF systems were preliminarily selected for more convenient and rapid experimental analysis of the mixtures.

Analysis of TEOS Solubility in EO

Previously,[35] the solubility of TEOS in various epoxy oligomers at high epoxy oligomer concentrations was studied using the cloud-point method. In addition, we used a similar method to determine the full solubility limits of TEOS/EO over the entire concentration range using light scattering and optical microscopy.

Fig. 2 shows the typical dependence of the scattered light intensity on temperature for a TEOS/EO mixture with a ratio of 25/75 (*V*/*V*): in the cooling mode from 75 °C to 5 °C (blue curve) and in the heating mode from 5 °C to 30 °C (red curve).

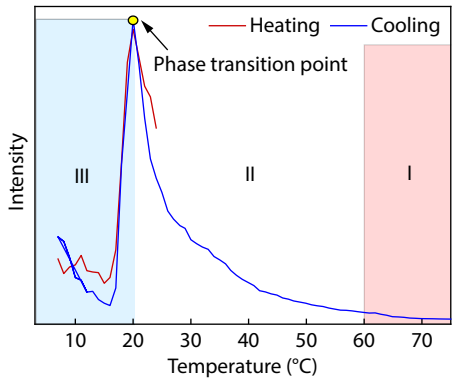

Fig. 2 Dependence of the change in light scattering intensity on temperature for a TEOS/EO mixture in a ratio of 25/75 (*V*/*V*).

The heated solution was homogeneous and did not scatter any light. As it cools, the morphology of the solution changes, which leads to a change in light scattering. Three regions of macroparticle formation in the TEOS/EO system can be distinguished in the given dependence. The first is a quasi-linear region at temperatures from 75 °C to 60 °C, corresponding to the existence of the solution. The second is a transition region from 60 °C to 20 °C, corresponding to the appearance of nuclei of a new phase and their growth, with a proportional increase in the intensity of light scattering in the system. This stage ends with a critical point at which a regime of concentration fluctuations and phase separation kinetics consistent with spinodal-type phase separation occurs, in accordance with article by Chalykh, A. E. *et al.*[71] The third is the region of aggregate particle formation. Macroseparation of the mixture into two phases was observed: one was enriched in EO with dissolved TEOS and the other was enriched in TEOS with dissolved EO. In this case, the light scattering decreased sharply and did not change further with changing temperature.

The light-scattering data correlated well with the optical microscopy data. Cooling of a homogeneous TEOS/EO solution resulted in the formation of an emulsion. Depending on the component ratio, both direct and reverse emulsions can be formed, with a transition point occurring at a TEOS/EO ratio of 1:1. This process is reversible and can easily be reproduced by cyclic heating. Examples of these solutions and emulsions are shown in Fig. 3.

Fig. 3 shows that at 25 °C, the TEOS/EO mixture exhibited macrophase separation. The two equilibrium phases formed emulsions with different TEOS droplet sizes in the EO. When the emulsion was heated above the upper critical solution temperature (UCST), the mixture formed a solution. When the

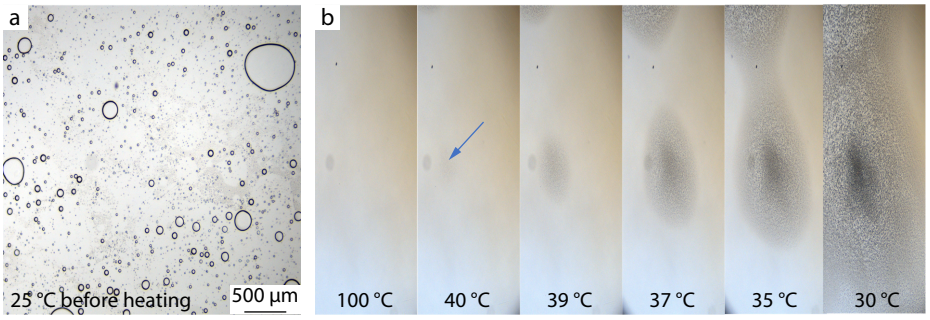

Fig. 3 TEOS/EO system solutions and emulsions micrographs in a ratio of 47/53 depending on the change in the medium temperature: (a) before heating, (b) after heating to 100 °C with gradual cooling at a constant rate.

cell is cooled to 40 °C, the system begins to exhibit the first signs of phase separation (indicated by the blue arrow): small TEOS droplets form. As the mixture temperature decreased further, the number of TEOS droplets increased, and localized areas of the emulsions merged, starting at 35 °C, while the TEOS droplet size remained unchanged.

Fig. 4 clearly shows that the TEOS/EO solution with a ratio of 25/75 was homogeneous, while the concentration of 31/69 formed an emulsion.

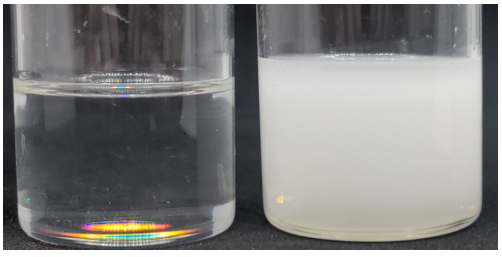

Fig. 4 Photographs of solutions and emulsions of the TEOS/EO system with different component ratios at 25 °C.

The critical points obtained using optical microscopy and dynamic light scattering were plotted on the phase diagram of the TEOS/EO system (Fig. 5).

Optical interferometry was used to analyze the phase state of the TEOS/EO binary system. Interdiffusion of the components was studied in the temperature range of 25–55 °C. The typical interferograms are shown in Fig. 6. Initially, a phase boundary was observed in the contact zone of the components (Fig. 6a), with bends in the interference fringes observed on both sides. This indicates the interdiffusion of TEOS and EO. Ten minutes after contact between the components,

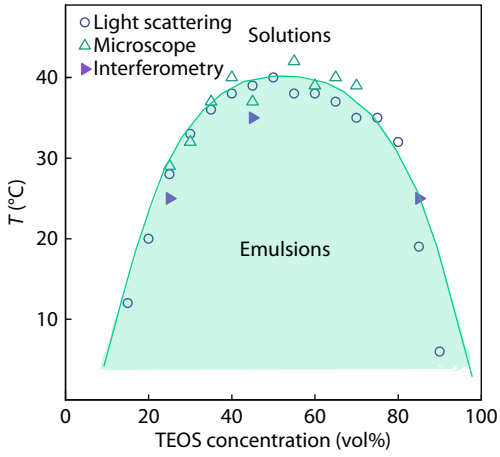

Fig. 5 Phase diagram of the TEOS/EO system.

the diffusion front expanded, and the boundary disappeared, indicating complete dissolution of the EO in TEOS (Fig. 6b).

A series of interferograms were obtained at different temperatures. The calculated boundary concentrations of the components were plotted in a phase diagram (Fig. 5).

The phase behavior of the TEOS/EO binary system is characterized by amorphous separation at an upper critical solution temperature (UCST). Complete component compatibility was achieved at temperatures above the UCST. Below the UCST, the system is separated into two heterogeneous phases. The solubilities of the components increased with increasing temperature.

Interdiffusion coefficients were determined for the TEOS/EO system.[26,72,73] The typical concentration dependence is shown in Fig. 7. The obtained curve is typical for systems with complete component compatibility.[48,50] The diffu-

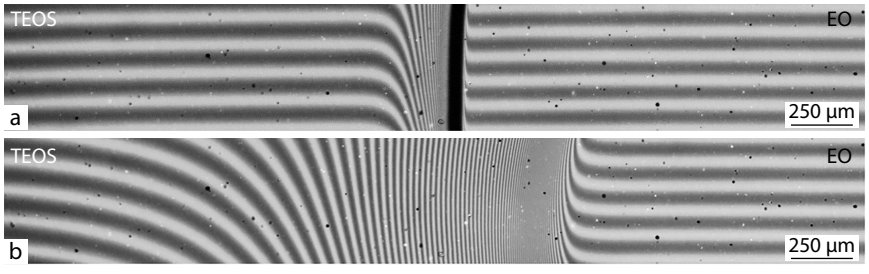

Fig. 6 Interferograms of the diffusion zone in the TEOS/EO system recorded (a) 5 s and (b) 10 min after the components were brought into contact. *T*=55 °C.

https://doi.org/10.1007/s10118-026-3783-6

sion coefficient changed smoothly with a change in the component concentration. Translational mobility in TEOS/EO solutions decreases with increasing oligomer concentration, which, in this case, is determined by a significant difference in the viscosity coefficients of the components.

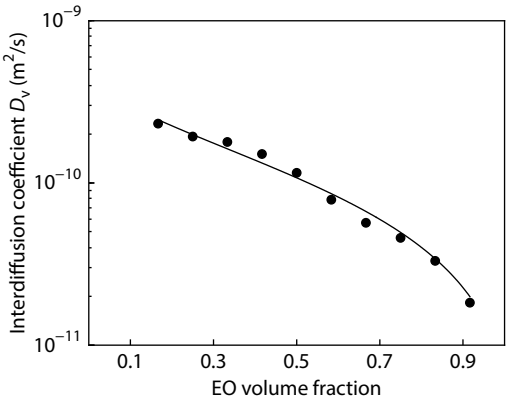

Fig. 7 Concentration dependence of the interdiffusion coefficient for the TEOS/EO system at 55 °C.

Compatibility of Three-component Systems EO/TEOS/PSF

Numerous studies on systems based on epoxy oligomers and polysulfones of various grades have shown that such systems are characterized by amorphous separation with a UCST.[25,50,72] The system under study behaved in a similar manner. Interferometry revealed the temperature-dependent miscibility of the PSF/EO system. At 100 °C, a residual interdiffusion boundary is still observed (Fig. 8a), indicating a partially mixed state. A fully developed continuous diffusion zone, corresponding to a single-phase state, was achieved only at higher temperatures (Fig. 8b, 200 °C), consistent with UCST-type phase behavior. The typical interferograms are shown in Fig. 8. At temperatures below the UCST, the components exhibit limited compatibility (Fig. 8a, zone I); the interferogram shows a phase boundary and bends of fringes on both sides, indicating the diffusion of PSF into EO and EO into PSF. At temperatures above the UCST, the phase boundary disappears and a continuous diffusion zone can be observed in the interferogram (Fig. 8b, zone II), indicating a transition toward a single-phase state of PSF and EO.

When cooled to room temperature, all the studied PSF/EO systems remained kinetically stable during the observation period without detectable phase separation (at least a week). This behavior can be attributed to the high viscosity of the resulting solutions, where solution stabilization occurs because of the limited mobility of the large oligomer that penetrates the swollen polysulfone macromolecule upon heating.

The phase states of the ternary systems were assessed by optical microscopy and interferometry. In the case of optical microscopy, the phase separation process was recorded by the onset of the second-phase droplet appearance upon slow cooling of the system. Figs. 9(a) and 10(a) show that a system with a TEOS content of 23 vol% is homogeneous over a wide temperature range (from 25 °C to 200 °C). A similar result was observed for the systems with a TEOS concentration of 26 vol% (Figs. 9b and 10b). An increase in the TEOS concentration in the ternary system (68/28.5/3.5) led to phase separation, even at elevated temperatures (Fig. 9c, 100 °C). Upon cooling the mixture, the separation became more pronounced, which was indicated by an increase in the number of droplets per unit volume (Fig. 9c, 25 °C) and turbidity of the

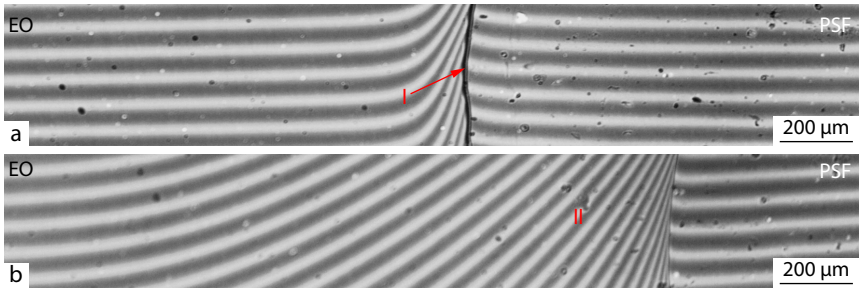

Fig. 8 Interferograms of the PSF/EO system interdiffusion zone at (a) 100 °C and (b) 200 °C.

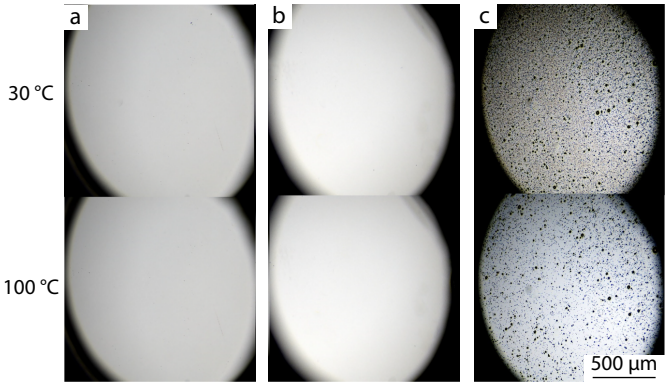

Fig. 9 Systems micrographs with concentrations: (a) 73/23/4, (b) 70/26/4, (c) 68/28.5/3.5 depending on the change in the medium temperature.

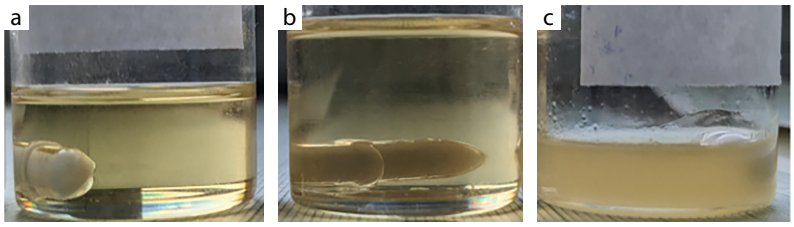

Fig. 10 Systems with different EO/TEOS/PSF contents (vol%): (a) 73/23/4, (b) 70/26/4, (c) 68/28.5/3.5. *T*=25 °C.

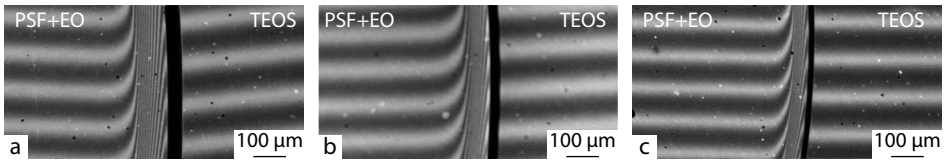

Fig. 11 Interferograms of the diffusion zone between TEOS and the PSF/EO solutions 30 min after contact: (a) 5 vol% PSF, (b) 10 vol% PSF, (c) 15 vol% PSF. *T*=25 °C.

transparent solution (Fig. 10c).

Interferometry was used to evaluate the diffusion of TEOS into the PSF/EO solutions containing 5 vol%, 10 vol%, and 15 vol% of the thermoplastic. At 25 °C, the interferograms clearly show the interface (Fig. 11). Bends in the interference fringes were observed on the side of the PSF/EO solution, indicating unidirectional diffusion of TEOS into the PSF/EO system. The diffusion intensity decreased with increasing PSF content in the EO, as illustrated by the movement of the isoconcentration planes (Fig. 12). The decrease in translational mobility occurs primarily owing to an increase in the PSF proportion and, consequently, an increase in the viscosity of the system.

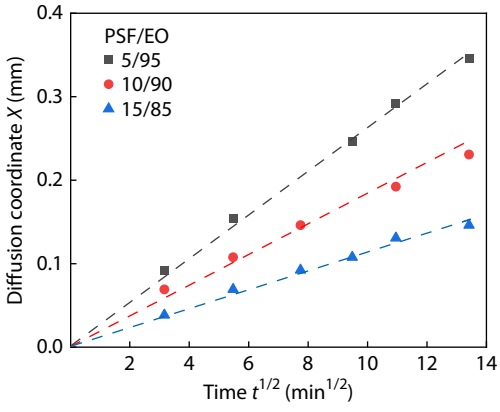

Fig. 12 Movement of isoconcentration planes in the system (TEOS-PSF/EO solution). *T*=25 °C.

The shift in the isoconcentration planes over time is almost linear. For the system under study, a dependence is observed that can be described by equation:[74]

$$X \approx k \cdot t^{0.5} \quad (2)$$

where X is the penetration depth of the diffusing component, k is a constant associated with the diffusion coefficient.

This is typical for diffusion mixing of components, which is not complicated by the simultaneous occurrence of chemical processes.[48,72]

At elevated temperatures, the interdiffusion processes in the PSF/EO and TEOS systems are more intense. This is reflected in the interference pattern as an expansion of the diffusion zones (Zone II) (Fig. 13). However, these components were only partially compatible. Phase separation was observed in the contact zone between the components; when TEOS was added to the PSF/EO system, the polymer precipitated from the solution (Zone I).

In addition to analyzing the interaction of the PSF solution with the TEOS solvent in the epoxy oligomer, the effect of adding the solvent (TEOS, 25 vol%) to the epoxy oligomer and the interaction of the resulting mixture with PSF were assessed. Fig. 14 shows the interference patterns of the contact zone of the components for the PSF/EO and EO/TEOS/PSF systems obtained at 100 °C.

The addition of TEOS increased the diffusion rate. The calculated interdiffusion coefficients are shown in Fig. 15. The calculations of the interdiffusion coefficients based on the experimentally determined concentration distribution curves are based on a model in which diffusion occurs between two contacting semi-infinite media. The numerical values of the limiting partial diffusion coefficient, D_v, were calculated according to Fick's law:

$$D_v = \frac{1}{2}\left(\frac{X}{t^{0.5}}\right)^2 \quad (3)$$

where X is the penetration depth of the diffusing component and t is the observation time.

The obtained diffusion coefficients should be considered as apparent values that describe effective mass transport in the ternary system. The EO/TEOS/PSF system is characterized by a higher diffusion mobility than that of the PSF/EO system. This can be explained by the presence of TEOS and, consequently, a decrease in the viscosity of the system. The onset temperature of diffusion in the EO/TEOS/PSF system was several degrees lower than that in the PSF/EO binary mixture.

Based on the data obtained by optical microscopy and interferometry, a phase diagram was constructed, and the regions of existence of the emulsions and solutions of the three-component EO/TEOS/PSF systems were determined (Fig. 16).

At 25 °C (Fig. 16a), we can observe that blends with a TEOS contents above 20% and 15% PSF blends with a TEOS con-

https://doi.org/10.1007/s10118-026-3783-6

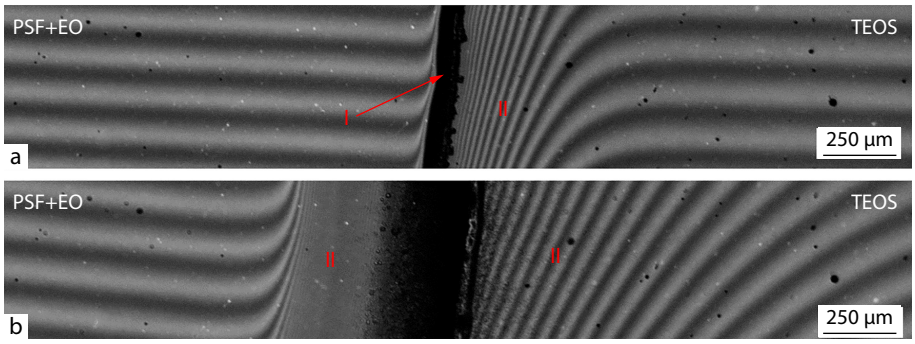

Fig. 13 Interferogram of the diffusion zone of the TEOS system and the PSF/EO 5/95 solution after (a) 10 s and (b) 5 min after the start of contact between the components. *T*=80 °C.

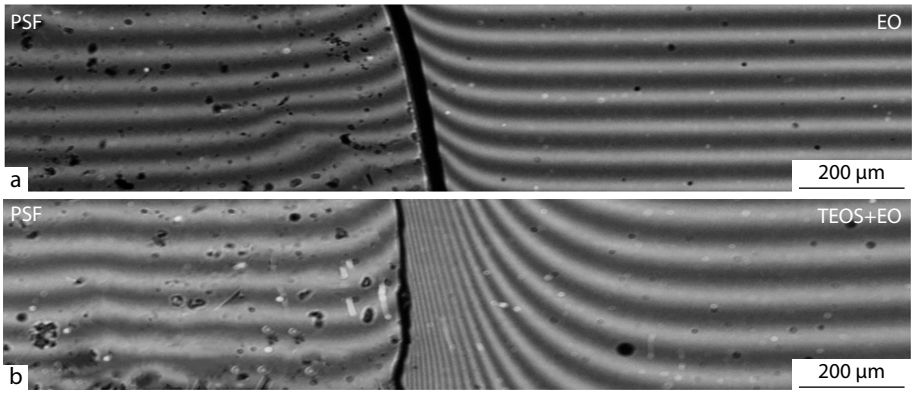

Fig. 14 Interferograms of the diffusion zone of systems: (a) PSF/EO and (b) PSF with TEOS/EO 25/75 solution. *T*=100 °C.

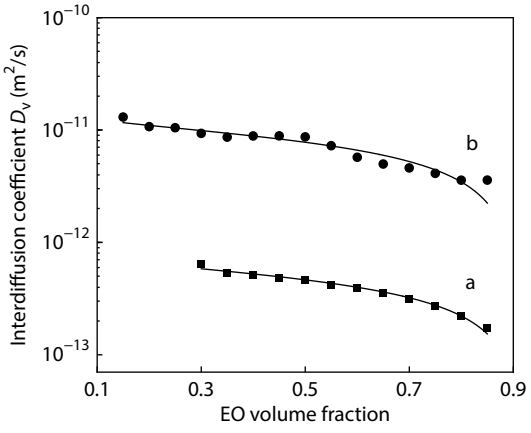

Fig. 15 Concentration dependence of the interdiffusion coefficient for the systems (a) PSF/EO and (b) EO/TEOS/PSF. *T*= 100 °C.

tents above 10% are emulsions (pink area) with the exception of EO/TEOS/PSF blends with compositions of 81/5/14, 87/3/10, 78/13/9, and 79/17/4.

At lower concentrations of TEOS and PSF in the epoxy matrix, the probability of solution formation is higher. The maximum concentration of a homogeneous stable solution with high PSF and TEOS contents was 77/9/14.

At 100 °C (Fig. 16b), component compatibility increased, as expected. The emulsion zone decreased (pink area). Under these conditions, ternary systems with increased PSF and TEOS content were possible. The EO/TEOS/PSF 63/16/21 and EO/TEOS/PSF 61/15/24 systems are stable solutions.

Thus, the solution existence regions with the maximum TEOS and PSF contents in the system were determined. The conditions for producing highly concentrated fluid PSF solutions in EO containing more than 30% PSF relative to EO and 15% TEOS per mixture were determined. This opens the possibility of developing highly filled polymer-oligomer binders containing silicon dioxide nanoparticles after curing the epoxy oligomer and performing the hydrolytic polycondensation of TEOS.

To evaluate the effect of TEOS on the rheological behavior of the highly concentrated EO/PSF systems, the frequency dependence of the complex viscosity was measured for a PSF/EO binary blend and three EO/TEOS/PSF ternary compositions located in the homogeneous region of the phase diagram (Fig. 17).

These results demonstrate that the introduction of TEOS leads to a substantial decrease in viscosity while preserving a high polysulfone concentration in the system. In particular, the compositions located near the phase-stability boundary exhibited significantly lower viscosities than the highly concentrated binary PSF/EO solution (EO/PSF = 80/20, *V*/*V*). The reduction in viscosity is attributed to the low viscosity of TEOS and is consistent with the increased diffusion mobility observed in interferometric experiments (Figs. 12 and 15).

Thus, the addition of TEOS enables the preparation of homogeneous EO/TEOS/PSF systems containing high concentrations of polysulfone, while maintaining rheological characteristics that are more favorable for processing.

https://doi.org/10.1007/s10118-026-3783-6

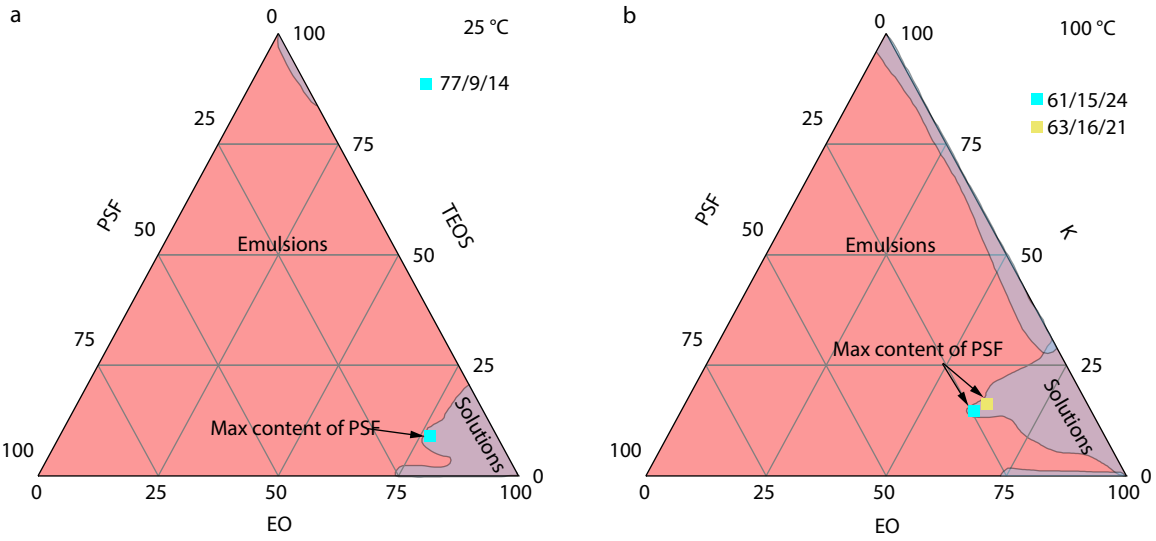

Fig. 16 Three-component phase diagram of EO/TEOS/PSF: (a) 25 °C, (b) 100 °C.

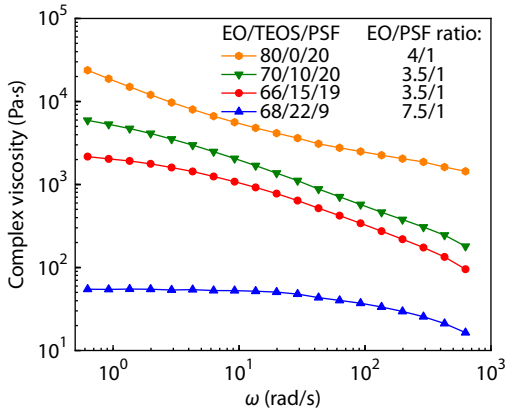

Fig. 17 Frequency dependence of complex viscosity for EO/PSF and EO/TEOS/PSF systems with high PSF content.

CONCLUSIONS

The phase states of binary and ternary systems based on epoxy oligomers containing polysulfone and tetraethoxysilane were studied. The compatibility parameters of the PSF, EO, and TEOS components were calculated theoretically using the Hansen method. Based on the calculated RED values, the compatibility of the two-component PSF-EO and TEOS-EO systems was determined (RED < 1). For the PSF-TEOS pair, the obtained parameter value exceeded unity, indicating the absence of interaction in this system.

Phase diagrams were constructed for the binary TEOS/EO and ternary EO/TEOS/PSF systems using dynamic light scattering, optical microscopy, and interferometry. The regions of existence of a homogeneous solution of the EO/TEOS/PSF system were determined. The optimum polymer and active diluent concentrations were determined to achieve a high PSF content in the mixture while maintaining the overall low viscosity of the system. Compositions containing TEOS were identified as the highest-PSF homogeneous formulations within the studied concentration range and exhibited substantially reduced viscosity compared to the corresponding binary PSF/EO systems.

The main determining factor for compatibility in the EO/TEOS/PSF system is the TEOS concentration as well as the temperature regime, which significantly expands the homogeneity range. The obtained data provide a basis for controlling the phase behavior of multicomponent systems.

Conflict of Interests

The authors declare no interest conflict.

ACKNOWLEDGMENTS

This work was financially supported by the State Program of A.V. Topchiev Institute of Petrochemical Synthesis, RAS (TIPS RAS).

REFERENCES

1 Fekiač, J. J.; Krbata, M.; Kohutiar, M.; Janík, R.; Kakošová, L.; Breznická, A.; Eckert, M.; Mikuš, P. Comprehensive review: optimization of epoxy composites, mechanical properties, & technological trends. *Polymers* **2025**, *17*, 271.
2 Luo, L.; Zhang, F.; Leng, J. Shape memory epoxy resin and its composites: from materials to applications. *Research* **2022**, *2022*, 9767830.
3 Liang, M.; Liu, X.; Liu, D.; Li, X.; Hu, X.; Feng, C.; Li, T.-T.; Lin, J.-H.; Chang, B.; Chen, J. A review of the curing rate and mechanical properties of epoxy resin on polymer matrix composites. *J. Polym. Res.* **2024**, *31*, 337.
4 Mousavi, S. R.; Estaji, S.; Paydayesh, A.; Arjmand, M.; Jafari, S. H.; Nouranian, S.; Khonakdar, H. A. A review of recent progress in improving the fracture toughness of epoxy-based composites using carbonaceous nanofillers. *Polym. Compos.* **2022**, *43*, 1871–1886.
5 Gonçalves, F. A. M. M.; Santos, M.; Cernadas, T.; Alves, P.; Ferreira, P. Influence of fillers on epoxy resins properties: a review. *J. Mater. Sci.* **2022**, *57*, 15183–15192.
6 Zhang, J.; Zhang, Z.; Huang, R.; Tan, L. Advances in toughening modification methods for epoxy resins: a comprehensive review. *Polymers* **2025**, *17*, 1288.

Graphical Abstract

Phase Equilibrium Analysis of Ternary Systems Based on an Epoxy Oligomer, Polysulfone, and Tetraethoxysilane

Ivan M. Obidin, Maria V. Mironova, and Ivan Yu. Skvortsov

Russian Academy of Sciences, Russian Federation

The regions of existence of a homogeneous solution of the epoxy oligomer/tetraethoxysilane/polysulfone (EO/TEOS/PSF) ternary system were determined. The obtained data provide a basis for controlling the phase behavior of multicomponent systems based on epoxy oligomers.

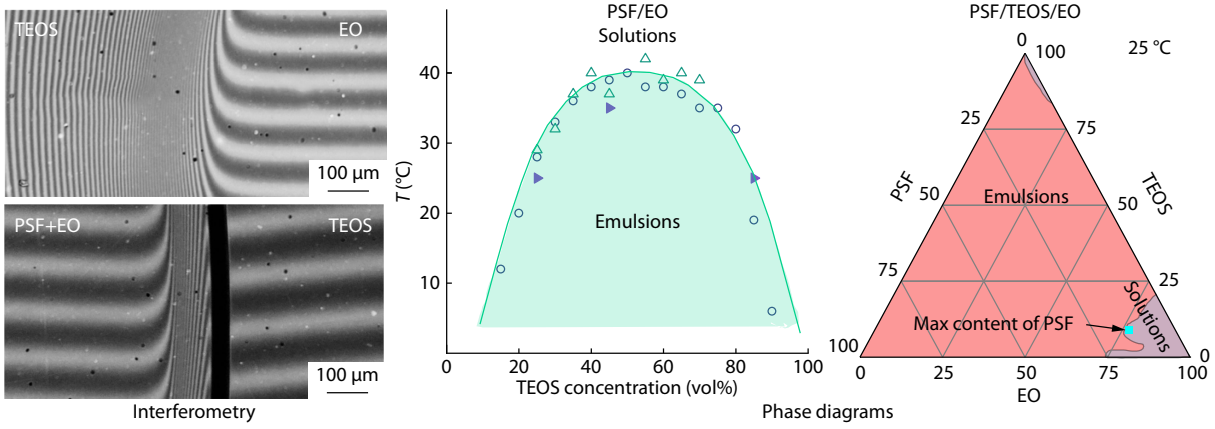

Chinese J. Polym. Sci. 2026 *https://doi.org/10.1007/s10118-026-3783-6*

7 Sun, S.; Yu, Q.; Yu, B.; Zhou, F. New progress in the application of flame-retardant modified epoxy resins and fire-retardant coatings. *Coatings* **2023**, *13*, 1663.
8 Wang, S.; Cao, M.; Xue, H.; Cong, F.; Li, X.; Zhao, C.; Su, W. Nano-silica reinforced epoxy resin/nano-rubber composite material with a balance of stiffness and toughness. *High Perform. Polym.* **2021**, *33*, 685–694.
9 Yu, B.; Zhang, Y.; Liu, Y.; Jin, Y.; Song, Y.; Peng, M. Enhancing the mechanical properties of carbon fiber/epoxy resin laminates through a combination of carbon fiber coating and matrix reinforcement with an aminated para-polyamide. *Compos. Part A: Appl. Sci. Manuf.* **2025**, *191*, 108740.
10 Deng, E.; Dai, X.; Zhang, L.; Zheng, T.; Liu, X.; Shen, J. High-efficient toughening and strengthening of epoxy resin with organic-inorganic core-shell nanoparticles. *Compos. Part A: Appl. Sci. Manuf.* **2025**, *198*, 109113.
11 Hao, Q.; Liu, S.; Wang, X.; Zhang, P.; Mao, Z.; Zhang, X. Progression from graphene and graphene oxide to high-performance epoxy resin-based composite. *Polym. Degrad. Stab.* **2024**, *223*, 110731.
12 Karthikeyan, L.; Robert, T. M.; Desakumaran, D.; Balachandran, N.; Mathew, D. Epoxy terminated, urethane-bridged poly (ether ether ketone) as a reactive toughening agent for epoxy resins. *Int. J. Adhes. Adhes.* **2022**, *112*, 102983.
13 Rehman, M. M.; Shaker, K.; Nawab, Y. Influence of polyether ether ketone particles on thermal characteristics of carbon/epoxy composite. *J. Therm. Anal. Calorim.* **2023**, *148*, 6003–6011.
14 Zheng, T.; Xi, H.; Wang, Z.; Zhang, X.; Wang, Y.; Qiao, Y.; Wang, P.; Li, Q.; Li, Z.; Ji, C.; Wang, X. The curing kinetics and mechanical properties of epoxy resin composites reinforced by PEEK microparticles. *Polym. Test.* **2020**, *91*, 106781.
15 Tretyakov, I. V.; Petrova, T. V.; Kireynov, A. V.; Korokhin, R. A.; Platonova, E. O.; Alexeeva, O. V.; Gorbatkina, Yu. A.; Solodilov, V. I.; Yurkov, G. Yu.; Berlin, A. A. Fracture of epoxy matrixes modified with thermo-plastic polymers and winding glass fibers reinforced plastics on their base under low-velocity impact condition. *Polymers* **2023**, *15*, 2958.
16 Tretyakov, I. V.; Vyatkina, M. A.; Cherevinskiy, A. P.; Solodilov, V. I.; Shapagin, A. V.; Korokhin, R. A.; Budylin, N. Yu.; Kireinov, A. V.; Gorbatkina, Yu. A. Effect of polyethersulfone on the properties of epoxy resin and wound unidirectional glass fiber reinforced plastics based on it. *Bull. Russ. Acad. Sci. Phys.* **2021**, *85*, 876–880.
17 Sopotov, R. I.; Zyukin, S. V.; Gorbunova, I. Yu.; Tuzova, S. Yu. The rheokinetics of the curing of epoxy oligomer ED-20 modified with polysulphone and polyesterimide. *Int. Polym. Sci. Technol.* **2016**, *43*, 7–10.
18 Girard-Reydet, E.; Vicard, V.; Pascault, J. P.; Sautereau, H. Polyetherimide-modified epoxy networks: Influence of cure conditions on morphology and mechanical properties. *J. Appl. Polym. Sci.* **1997**, *65*, 2433–2445.
19 Gorbunova, I. Yu.; Shustov, N. V.; Kerber, M. L. Influence of thermoplastic modifiers on the properties and the process of curing of epoxy polymers. *J. Eng. Phys. Thermophys.* **2003**, *76*, 572–576.
20 Polunin, S. V.; Gorbunova, I. Yu.; Kerber, M. L. Properties of epoxy matrix modified with boron nitride. *Polym. Sci. Ser. D* **2024**, *17*, 745–747.
21 Wang, D.; Guo, Z.; Zhao, L.; Li, H.; Liu, C.; Zhang, G.; Xiao, W.; Zheng, S.; Su, K.; Zhang, Y.; Li, B. Mechanical properties, thermal

stability, and phase structure of polysulfone toughened epoxy structural adhesive. *J. Appl. Polym. Sci.* **2025**, *142*, e57574.
22 Sun, Z.; Xu, L.; Chen, Z.; Wang, Y.; Tusiime, R.; Cheng, C.; Zhou, S.; Liu, Y.; Yu, M.; Zhang, H. Enhancing the mechanical and thermal properties of epoxy resin via blending with thermoplastic polysulfone. *Polymers* **2019**, *11*, 461.
23 Dzhangurazov, E. B.; Petrova, T. V.; Shapagin, A. V.; Tretyakov, I. V.; Korokhin, R. A.; Kireynov, A. V.; Alexeeva, O. V.; Solodilov, V. I.; Yurkov, G. Yu.; Berlin, A. A. Fracture toughness of winding carbon plastics based on epoxy matrices and reinforced by polysulfone film. *Polymers* **2025**, *17*, 220.
24 Yuan, Q.; Wang, Z.; Yao, H.; Huang, J.; Zuo, S.; Huang, H. Comparative study of reactive diluents with different molecular structures on the curing properties of epoxy adhesives and the interface bonding properties with mortar. *Int. J. Adhes. Adhes.* **2023**, *126*, 103473.
25 Ponomarenko, A. D.; Nikulova, U. V.; Shapagin, A. V. Phase equilibria and interdiffusion in the ternary system epoxy oligomer-polysulfone-alkyl glycidyl ether. *Polymers* **2024**, *16*, 130.
26 Petrova, T. V.; Tretyakov, I. V.; Kireynov, A. V.; Shapagin, A. V.; Budylin, N. Yu.; Alexeeva, O. V.; Beshtoev, B. Z.; Solodilov, V. I.; Yurkov, G. Yu.; Berlin, A. A. Structure and properties of epoxy polysulfone systems modified with an active diluent. *Polymers* **2022**, *14*, 5320.
27 Qiao, J.; He, J.; Lv, Y.; Yang, W.; Wang, K.; Huang, S.; Xu, K. The effect of different active diluents on the properties of epoxy materials. *J. Phys.: Conf. Ser.* **2024**, *2783*, 012027.
28 Petrova, T. V.; Tretyakov, I. V.; Solodilov, V. I. Technological parameters of epoxypolysulphone binders modified with furfuryl glycidyl ether. *Russ. J. Phys. Chem. B* **2023**, *17*, 177–181.
29 Liu, F.; Guo, K.; Yuan, J. Preparation of the modified epoxy resins with flexible diglycidyl ether of diethylene glycol. *High Perform. Polym.* **2014**, *26*, 326–334.
30 Li, C.; Liu, M.-H.; Liu, Z.-Y.; Qing, M.-L.; Wang, G. DSC and curing kinetics of epoxy resin using cyclohexanediol diglycidyl ether as active diluents. *J. Therm. Anal. Calorim.* **2014**, *116*, 411–416.
31 Malburet, S.; Bertrand, H.; Richard, C.; Lacabanne, C.; Dantras, E.; Graillot, A. Biobased epoxy reactive diluents prepared from monophenol derivatives: effect on viscosity and glass transition temperature of epoxy resins. *RSC Adv.* **2023**, *13*, 15099–15106.
32 Kurbatov, V. G.; Pugacheva, T. A.; Malkov, G. V.; Krasikova, M. S.; Golikov, I. V.; Il'in, A. A. Effect of active diluents on properties of epoxy compounds and coatings based on them. *Russ. J. Appl. Chem.* **2020**, *93*, 1340–1348.
33 Wang, D.; Wang, X.; Han, K.; Wang, D.; Yao, Z.; Yu, M.; He, Q.; Zhang, G. Effects of reactive diluent on processing, structure, and properties of epoxy foams and their sandwich composites. *Polym. Eng. Sci.* **2024**, *64*, 2073–2081.
34 Jagtap, A. R.; More, A. Developments in reactive diluents: a review. *Polym. Bull.* **2022**, *79*, 5667–5708.
35 Skvortsov, I. Y. Study of the influence of the sol-gel process of hydrolytic polycondensation of alkoxysilanes on the structure and properties of composites based on curable thermosetting binders. Thesis, Lomonosov Moscow State Academy of Fine Chemical Technology, **2011**.
36 Cheng, H.; Yin, Y.; Meng, W.; Liu, A.; Peng, L. Performance of epoxy resin composites reinforced with SiC modified by hydroxyl silane coupling agents. *Chem. Select* **2025**, *10*, e02509.
37 Taieh, N. K.; Hakeem, H. S.; Kadhim, M. S.; Mejbel, M. K.; Abdullah, I. T.; Al-Attabi, R.; Al-Khafaji, Z. S.; Nassir, M. H.; Idan, I. J.; Faris, A. N. Optimizing mechanical performance in woven basalt fibers/epoxy composites: Using silane coupling agents to modify epoxy resin for fiber-matrix interface. *J. Inorg. Organomet. Polym. Mater.* **2025**, *35*, 680–696.
38 Lin, X.; Chen, X.; Zhao, S.; Dou, B.; Peng, Q.; Deng, Z.; Wang, B.; Dong, C.; Chen, H.; Ren, M. Effect of silane-modified fluorinated graphene on the anticorrosion property of epoxy coating. *J. Appl. Polym. Sci.* **2023**, *140*, e53637.
39 Branda, F.; Grappa, R.; Costantini, A.; Luciani, G. Sol-gel approach for fabricating silica/epoxy nanocomposites. *Polymers* **2023**, *15*, 2987.
40 Skvortsov, I. Yu.; Varfolomeeva, L. A.; Kulichikhin, V. G. The effect of tetraethoxysilane on the phase state, rheological properties, and coagulation features of polyacrylonitrile solutions. *Colloid J.* **2019**, *81*, 165–175.
41 Sato, Y.; Sugimoto, A.; Iwashina, T.; Hayami, R.; Yamamoto, K.; Gunji, T. Hydrolysis and condensation behavior of tetraethoxysilane, hexaethoxydisiloxane, and octaethoxytrisiloxane. *J. Sol-Gel Sci. Technol.* **2023**, *108*, 377–391.
42 Shao, Q.; Pei, C.; Jin, M.; Ding, Y.; Chen, Z.; Kuang, T. Anchoring nanofillers at immiscible polymer interfaces enables strong, tough, high-output triboelectrics. *Nano Lett.* **2025**, *25*, 15895–15903.
43 Guo, H.; Ding, Y.; Lu, X.; Li, W.; Kuang, T. Precisely anchored amphiphilic metal-organic frameworks at polymer interfaces for robust biodegradable blends. *Chem. Mater.* **2025**, *37*, 7398–7409.
44 Skvortsov, I. Yu.; Kuzin, M. S.; Gerasimenko, P. S.; Mironova, M. V.; Golubev, Y. V.; Kulichikhin, V. G. Non-coagulant spinning of high-strength fibers from homopolymer polyacrylonitrile synthesized via anionic polymerisation. *Polymers* **2024**, *16*, 1185.
45 Mironova, M. V.; Tarasov, A. E.; Kuzin, M. S.; Skvortsov, I. Yu.; Arkharova, N. A.; Podval'naya, Yu. V.; Kulichikhin, V. G. Rheological and relaxational properties of mixed solutions based on linear and highly branched polyacrylonitrile. *Polym. Sci. Ser. A* **2022**, *64*, 354–365.
46 Robinson, C. Interferometric studies in diffusion. I. Determination of concentration distributions. *Proc. R. Soc. London, Ser. A* **1950**, *204*, 339–359.
47 Duda, J. L.; Sigelko, W. L.; Vrentas, J. S. Binary diffusion studies with a wedge interferometer. *J. Phys. Chem.* **1969**, *73*, 141–149.
48 Chalykh, A. E.; Sapozhnikova, I. N. Phase equilibria and mutual diffusion in polymer-polymer systems with chlorine-containing components. *Russ. Chem. Rev.* **1984**, *53*, 1062–1077.
49 Skvortsov, I. Y.; Kulichikhin, V. G.; Ponomarev, I. I.; Varfolomeeva, L. A.; Kuzin, M. S.; Razorenov, D. Y.; Zhigalina, O. M.; Khmelenin, D. N.; Kechek'yan, A. S. Some specifics of defect-free poly-(o-aminophenylene)naphthoylenimide fibers preparation by wet spinning. *Materials* **2022**, *15*, 808.
50 Shapagin, A. V.; Budylin, N. Yu.; Chalykh, A. E. Regulation of a phase structure at the interface in epoxy-polysulfone systems. *Russ. Chem. Bull.* **2018**, *67*, 2172–2177.
51 Makarov, I. S.; Golova, L. K.; Kuznetsova, L. K.; Bondarenko, G. N.; Skvortsov, I. Yu.; Mironova, M. V.; Platonov, V. A.; Bermeshev, M. V.; Gromov, A. V. Composite fibers based on cellulose and tetraetoxysilane: Preparation, structure and properties. *Fibre Chem.* **2017**, *49*, 101–107.
52 Lin, H.-M.; Nash, R. A. An experimental method for determining the Hildebrand solubility parameter of organic nonelectrolytes. *J. Pharm. Sci.* **1993**, *82*, 1018–1026.
53 Bhamare, V. G.; Joshi, R. R.; Gangurde, M. S.; Pawar, V. V. Theoretical consideration of solubility by Hildebrand solubility approach. *World J. Adv. Res. Rev.* **2021**, *12*, 528–541.
54 Zalamena, G.; Lopes, T. J.; Lucas, E. F.; Ramos, A. C. S. The Hildebrand solubility parameter and its importance in the scientific and technological scenario of flow assurance operations. *Pet. Chem.* **2023**, *63*, 886–897.
55 Flory, P. J. Thermodynamics of high polymer solutions. *J. Chem. Phys.* **1942**, *10*, 51–61.
56 Klueppelberg, J.; Handge, U. A.; Thommes, M.; Winck, J.

Composition dependency of the Flory--Huggins interaction parameter in drug-polymer phase behavior. *Pharmaceutics* **2023**, *15*, 2650.
57 Hansen, C. M. Hansen solubility parameters: a user's handbook, 2nd ed.; CRC Press, Boca Raton, **2007**.
58 Skvortsov, I. Yu.; Kuzin, M. S.; Gerasimenko, P. S.; Kulichikhin, V. G.; Malkin, A. Ya. Role of small amounts of water in the gelation of polyacrylonitrile solutions in dimethyl sulfoxide: Rheology, kinetics, and mechanism. *Macromolecules* **2024**, *57*, 3647−3663.
59 Hu, Y.; Sreeram, A.; Xia, W.; Wang, H.; Zhou, L.; Si, W.; Chen, Y.; Wu, P.; Liu, G. Use of Hansen solubility parameters (HSP) in the selection of highly effective rejuvenators for aged bitumen. *Road Mater. Pavement Des.* **2025**, *26*, 734−752.
60 Ethier, J.; Antoniuk, E. R.; Brettmann, B. Predicting polymer solubility from phase diagrams to compatibility: a perspective on challenges and opportunities. *Soft Matter* **2024**, *20*, 5652−5669.
61 Kuzin, M. S.; Skvortsov, I. Y.; Gerasimenko, P. S.; Subbotin, A. V.; Malkin, A. Ya. The role of the solvent nature in stretching polymer solutions (polyacrylonitrile spinning using different solvents). *J. Mol. Liq.* **2023**, *392*, 123516.
62 Patel, K. G.; Maynard, R. K.; Ferguson, L. S.; Broich, M. L.; Bledsoe, J. C.; Wood, C. C.; Coates, I.; Brettmann, B. Experimentally determined Hansen solubility parameters of biobased and biodegradable polyesters. *ACS Sustainable Chem. Eng.* **2024**, *12*, 2386−2393.
63 Chalykh, A. E.; Gerasimov, V. K.; Bukhteev, A. E.; Shapagin, A. V.; Kudryakova, G. K.; Brantseva, T. V.; Antonov, S. V.; Korokhin, R. A. Compatibility and phase structure evolution in polysulfone-curable epoxy oligomer blends. *Polym. Sci. Ser. A* **2003**, *45*, 676−685.
64 Medina Gonzalez, Y.; de Caro, P.; Thiebaud-Roux, S.; Lacaze-Dufaure, C. Fatty acid methyl esters as biosolvents of epoxy resins: A physicochemical study. *J. Solution Chem.* **2007**, *36*, 437−446.
65 Ning, N.; Qiu, Y.; Wei, Y. Building effective core/shell polymer nanoparticles for epoxy composite toughening based on Hansen solubility parameters. *Nanotechnol. Rev*. **2021**, *10*, 1183−1196.
66 Barabash, E.; Popov, Y.; Danchenko, Y. The study of the influence of chemical nature of functional groups in oligomeric and low-molecular modifiers on the rheological properties of the epoxy oligomer. *Chem. Chem. Technol.* **2021**, *15*, 53−60.
67 Tomić, M.; Dunjić, B.; Nikolić, M. S.; Maletaškić, J.; Pavlović, V. B.; Bajat, J.; Stevanović, J. Dispersion efficiency of montmorillonites in epoxy nanocomposites using solution intercalation and direct mixing methods. *Appl. Clay Sci.* **2018**, *154*, 52−63.
68 Maldonado-Lopez, L. E.; Fimbres-Weihs, G. A.; Escobar-Barrios, V. A. Structural modification of polysulfone/NMP membranes: effect of chloroform as co-solvent. *Polym. Bull.* **2022**, *79*, 6601−6615.
69 Milliman, H. W.; Boris, D.; Schiraldi, D. A. Experimental determination of Hansen solubility parameters for select POSS and polymer compounds as a guide to POSS-polymer interaction potentials. *Macromolecules* **2012**, *45*, 1931−1936.
70 Ghorani, B.; Russell, S. J.; Hebden, A. J.; Goswami, P. Single step assembly of biomolecule-loaded sub-micron polysulfone fibers. *Text. Res. J.* **2017**, *87*, 340−350.
71 Chalykh, A. E.; Gerasimov, V. K.; Mikhailov, Y. M. Diagrams of phase state of polymer systems, Yanus-K: Moscow, **1998**.
72 Shapagin, A. V.; Budylin, N. Yu.; Chalykh, A. E.; Solodilov, V. I.; Korokhin, R. A.; Poteryaev, A. A. Phase equilibrium, morphology, and physico-mechanics in epoxy-thermoplastic mixtures with upper and lower critical solution temperatures. *Polymers* **2021**, *13*, 35.
73 Chalykh, A. E.; Budylin, N. Yu.; Shapagin, A. V. Diffusion in epoxy oligomers and polymers. In *multifunctional epoxy resins: self-healing, thermally and electrically conductive resins*; Hameed, N., Capricho, J. C., Salim, N., Thomas, S., Eds.; Springer Nature, Singapore, **2023**, pp. 41−105.
74 Bazhanov, D. A.; Poteryaev, A. A.; Shapagin, A. V.; Shcherbina, A. A. Ethylene-vinyl acetate copolymers as potential thermoplastic modifiers of photopolymer compositions. *Polymers* **2023**, *15*, 131.